processes

Article

# Parametric Analysis and Optimization Design of the Twin-Volute for a New Type of Dishwasher Pump

Haichao Sun [1], Hui Xu [2], Yanjun Li [1], Xikun Wang [1] and Yalin Li [1,*]

[1] National Research Center of Pumps, Jiangsu University, 301 Xuefu Road, Zhenjiang 212013, China
[2] Ningbo FOTILE Kitchen Ware Co., Ltd., Ningbo 315336, China
* Correspondence: ylli@ujs.edu.cn

**Abstract:** To improve the hydraulic performance of a new type of dishwasher pump and solve the multi-parameter optimization problem, a genetic algorithm was introduced to optimize the special design of the twin-volute structure. Six curvature radii of the twin-volute structure were defined as the optimization parameters, and 100 groups of design samples were generated based on the Latin hypercube sampling (LHS) method. The pump head and the efficiency were taken as the optimization objectives, i.e., to improve the efficiency as much as possible while ensuring that the head would not be lower than 2 m. The important parameters were identified via sensitivity analysis, and the optimization problem was solved in detail by using the multi-objective genetic algorithm (MOGA). The results showed that the external profile of the first to the fourth section of the twin-volute structure had the most significant effect on the pump head and efficiency. The response surface method (RSM) was used to select the intervals of optimization, and a comparative simulation of the pump schemes before and after optimization was performed. The head curve did not significantly change before and after optimization. By contrast, the efficiency of the dishwasher pump significantly increased, showing an increase of 2.7% under the design point. Compared with the original model, the impeller of the optimal model pump had a lower overall distribution of turbulent kinetic energy, reduced the vorticity in the twin-volute inlet area, and increased the pressure in the flow channel. Our research results confirm that the combination of RSM and MOGA can effectively solve the problem of optimization for new types of dishwashers and can provide a reference for the development of subsequent hydraulic models.

**Keywords:** dishwasher pump; twin-volute; genetic algorithm; parametric analysis; optimization design



**Citation:** Sun, H.; Xu, H.; Li, Y.; Wang, X.; Li, Y. Parametric Analysis and Optimization Design of the Twin-Volute for a New Type of Dishwasher Pump. *Processes* **2023**, *11*, 305. https://doi.org/10.3390/pr11020305

Academic Editor: Fabricio Napoles-Rivera

Received: 27 October 2022
Revised: 12 December 2022
Accepted: 23 December 2022
Published: 17 January 2023



## 1. Introduction

In recent years, an increasing number of households use dishwashers. Traditional dishwashers, which are mostly built-in cabinet-type models, cannot accommodate all user needs. In order to save space, a sink-style dishwasher was designed and integrated into the conventional kitchen sink. Li et al. [1] compared the traditional dishwasher and a new sink-style dishwasher with an innovative pump, as shown in Figure 1, and it was found to be an important part of sink-style dishwashers. Its working principle is driven by the rotating effect of the impeller; the water enters the volute and initiates powerful torque for the passive rotation of the twin-volute to complete the water transmission and spraying function.

Some studies have addressed this new type of dishwasher pump. A numerical simulation study on the interaction between the impeller and the twin-volute structure in the dishwasher pump was carried out by Ning et al. [2]. Their results indicate that the hydraulic performance of the pump is slightly affected by the passive rotation of the twin-volute structure, which has a large effect on the flow field in the transition section located between the impeller and the volute. At the same time, a contrasting viewpoint on the vector distribution of the flow field was presented in this research paper. It was found that the shape of the vector distribution is the most regular for the 30 rpm scheme, which indicates that the stability of the pump is the highest. Zhu et al. [3] carried out experiments on the pressure pulsation of a dishwasher pump using twin-volute and single-volute schemes with passive rotation, and the experimental data were compared with the data of a single volute. Zhu et al. [4] analyzed the pressure pulsation characteristics of single-volute and twin-volute models in dishwasher pumps under stationary and rotating conditions. Both the experimental and numerical results showed that the pressure pulsation characteristics of the twin-volute scheme were better than those of the single volute and static volute. All the above studies guide innovation in the design of dishwasher pumps.

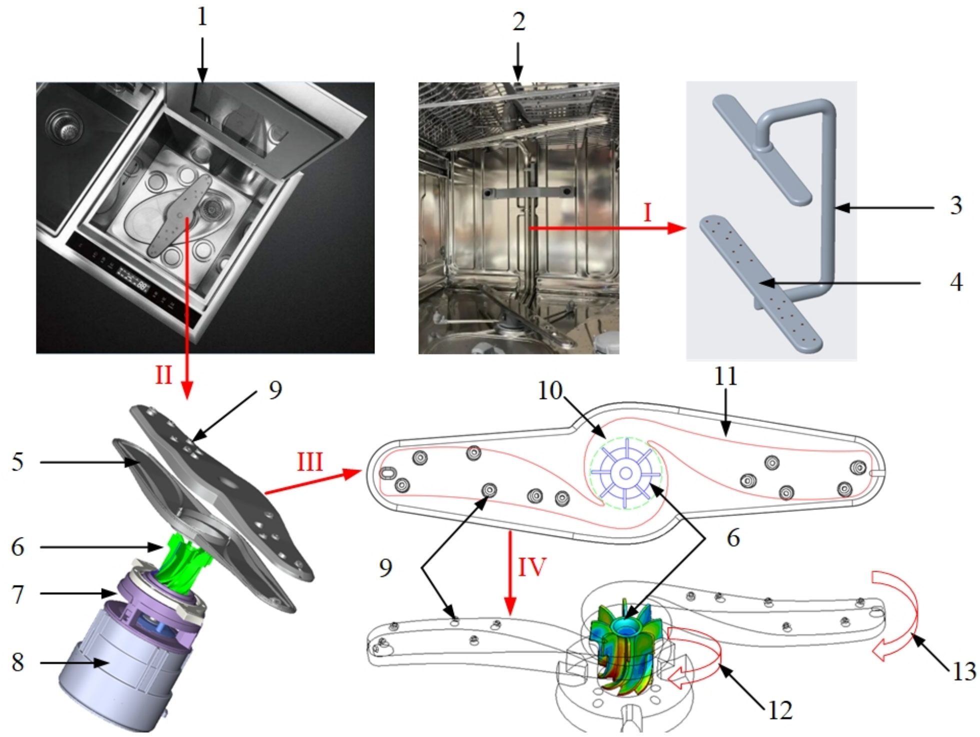


**Figure 1.** Comparison of new sink-type dishwasher with innovative pump and traditional dishwasher. I: spray and pipeline system of traditional dishwasher, II: new type of dishwasher pump, III: twin-volute spray arm, IV: computational domain of new type of dishwasher pump. 1: new sink-type dishwasher, 2: traditional dishwasher, 3: pipeline system, 4: traditional spray arm, 5: twin-volute, 6: compound impeller, 7: entrance section, 8: DC motor, 9: nozzle, 10: basic circle of volute, 11: profile of flow channel of twin-volute, 12: impeller active rotation, 13: volute passive rotation [1].

Numerous past researchers have investigated the volute since it is a crucial pump component for overcurrent conditions. By using experimental methods, Kaupert et al. [5] investigated the effect of the volute on the pressure field of a centrifugal impeller with a high specific speed. The pressure pulsation induced by the rotor–stator interaction between the rotating impeller and the stationary volute, as indicated by Hodkiewicz et al. [6] and CHU et al. [7], is a significant factor affecting the pump's performance. Numerous studies on pressure pulsation have been conducted [8–10]. Hakan et al. studied the three-dimensional course of a curved spray arm and its projection onto the plane [11]. This revolutionary curved design, which replaces the conventional spray arm, enhances the consumption of water and energy in dishwashers while enhancing their performance and reducing noise. Based on the stereoscopic light-curing molding technique, Dedoussis et al. [12] rebuilt and improved the spray arms in dishwashers, with various geometric designs. Studies have revealed that the throat area and the clearance between the impeller and the volute are significant factors affecting the hydraulic performance of the pump, and Wu [13] used CFD technology to analyze the effect of the geometry parameters of the volute on the performance of circulating hydraulic pumps, but the simulation was limited to those cases with few geometric models; thus, the study lacks research on the optimal design of the volute.

Studies focusing on the optimization process have extensively investigated the optimization of the characteristics of pump operation. Donno et al. designed centrifugal pump settings using genetic algorithms based on sophisticated surrogate optimization techniques and parameterized these settings using Bezier surfaces and Scilab scripts [14–16]. Finally, ERCOFTAC centrifugal pumps were used to verify the viability and efficacy of such optimization procedures. Thakkar et al. [17] optimized the clean centrifugal pump by using the response surface method and a multi-objective optimization algorithm. Their results showed that, in comparison to the original model, the head and efficiency of the optimization model at the design point increased by 9.154% and 10.15%, respectively. Lu et al. [18] used a radial basis function (RBF) neural network, the optimal Latin hypercube (OLH) sampling method, and the multi-island genetic algorithm to optimize mixed-flow pumps. Their CFD results revealed a 5.1% increase in efficiency. According to Zhao et al. [19], the performance of centrifugal pumps can be predicted by considering impeller characteristics using a non-parametric machine learning technique called Gaussian process regression (GPR). The outcomes demonstrated that the SE kernel function-equipped GPR model had a greater level of accuracy and resilience. Wang et al. [20] used the Latin hypercube sampling method (LHS) and a genetic algorithm (GA) to optimize the impeller in waste-heat discharge pumps, and they compared the precision of three additional models for pump performance prediction: the response surface model (RSM), the Kriging model (KRG), and the radial basis neural network (RBNN). Zhang et al. [21] studied the impact of rational pump blade shapes on pump hydraulic performance using proper orthogonal decomposition (POD); specifically, they applied the sum calculation method of NSGA-II and RBF to optimize its hydraulic performance, obtaining the Pareto optimal solution. An adaptive proper orthogonal decomposition (APOD) alternative model was put forth by Chen et al. [22]. The model was capable of making quick and precise predictions about the impeller's flow field. The forecast time was less than 1/360 of the time needed with CFD, and the prediction accuracy was noticeably better than that of the FPOD approach.

Although a few studies exist on this new type of volute structure, compared with the traditional volute, the influence of this special twin-volute structure on the hydraulic performance of the pump and its optimal design remains to be studied. Thus, in this paper, an optimization method is proposed that combines the RSM and MOGA for improving the hydraulic performance optimization of the new type of dishwasher pump. The RSM is applied to select the design parameter interval for the optimization. The head and efficiency of the new type of dishwasher pump are set as the optimization objectives. The best combination of design parameters is achieved by using the MOGA for the approximate model.

## 2. Numerical Simulation and Experimental Validation

### *2.1. Pump Model*

Figure 2 depicts the original geometric model of the new type of dishwashing pump. It is designed to deliver flow at a volumetric flow rate of 55 L/min, a head of 2 m, and a rotational speed of 3000 r/min. The geometrical parameters of the dishwasher pump are listed in Table 1.

Notably, the numerical twin-volute model is simplified compared with the real machine volute, and the two-dimensional profile of the numerical model is determined by six radii of curvature.

As shown in Figure 3, six curves with various curvature radii primarily regulate the twin-volute. Correspondingly, the outer curve of the twin-volute structure's cross-section consists of two curves with different radii of curvature, which are defined as the parameters "DS_1" and "DS_2", respectively; the inner curve of the cross-section is composed of three curves with various radii of curvature, and they are defined as "DS_3", "DS_4", and "DS_5"; the external profile of the first to the fourth section of the worm shell is defined as "DS_6".

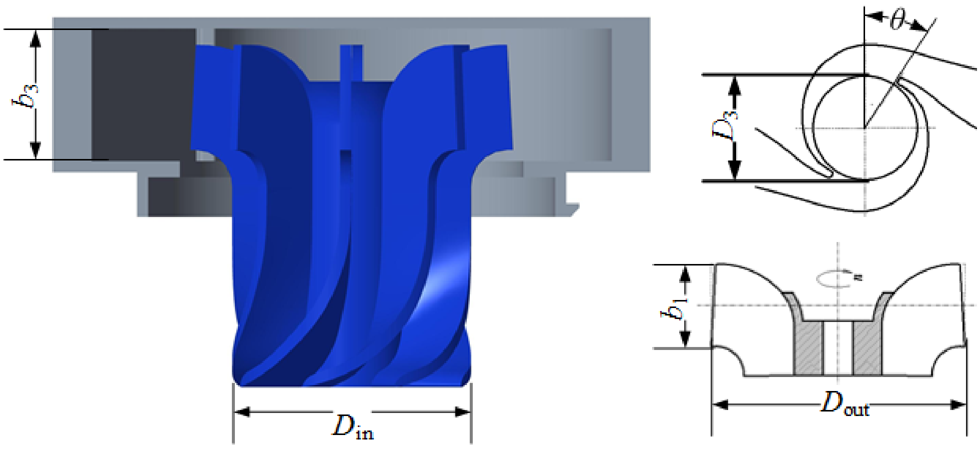


**Figure 2.** Numerical model of the new type of dishwasher pump [3].

**Table 1.** Parameters of new type dishwasher pump.

| Part | Parameter | Value |
|---|---|---|
| Impeller | Impeller inlet diameter $D_{in}$ (mm) | 32 |
| | Blade outlet width $b_1$ (mm) | 14.15 |
| | Impeller outlet diameter $D_{out}$ (mm) | 43.3 |
| | blade number $Z$ | 8 |
| Volute | Volute inlet width $b_3$ (mm) | 17.8 |
| | Base circle diameter $D_3$ (mm) | 46 |
| | Setting angle of tongue $\theta$ (°) | 34 |

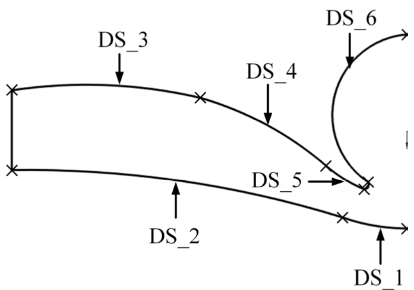


**Figure 3.** Cross-section of the twin-volute.

### *2.2. Mesh Independence*

The whole computational domain is composed of the inlet pipe, the impeller, and the twin volute. All the parts except for the inlet pipe were generated with an unstructured mesh using ANSYS Meshing software, and Figure 4 depicts these grids in more detail.

**Figure 4.** Mesh of the model pump.

To determine the most logical number of grids, grid independence was carried out. By altering the grid size while ensuring the grid quality, the dishwasher pump head with five groups of different grid numbers was calculated. Table 2 shows that, compared with Mesh 4, the change rate for the pump head using Mesh 5 was 0.18%. The head of Mesh 4 was found to have considerable accuracy, and the simulation changed a little even if the number of grids increased. Consequently, Mesh 4 was selected for numerical simulation throughout the optimization.

**Table 2.** Mesh independence verification of the original pump.

| Mesh | Inlet Pipe ($\times 10^4$) | Impeller ($\times 10^4$) | Volute ($\times 10^4$) | Total Grid ($\times 10^4$) | Head (m) | Error (%) |
|---|---|---|---|---|---|---|
| 1 | 8.33 | 89.24 | 105.23 | 202.8 | 2.053 | |
| 2 | 13.59 | 100.48 | 135.89 | 249.96 | 2.106 | 2.58 |
| 3 | 15.23 | 127.54 | 165.48 | 308.25 | 2.163 | 2.7 |
| 4 | 17.33 | 152.74 | 201.47 | 371.54 | 2.187 | 1.1 |
| 5 | 20.49 | 175.26 | 247.62 | 443.37 | 2.191 | 0.18 |

### 2.3. Turbulence Model

ANSYS Fluent was used to simulate the incompressible flow for the dishwasher pump. The continuity equation was solved using the SST $k$–$\omega$ published by Menter [23] because of its accurate predictions of the inception and quantum of flow separation under various pressure gradients. The governing equations can be expressed as follows:

$$\frac{\partial(\rho k)}{\partial t} + \frac{\partial(\rho k u_i)}{\partial x_i} = \frac{\partial}{\partial x_j}\left(\Gamma_k \frac{\partial k}{\partial x_j}\right) + G_k - Y_k + S_k \tag{1}$$

$$\frac{\partial(\rho \omega)}{\partial t} + \frac{\partial(\rho \omega u_i)}{\partial x_i} = \frac{\partial}{\partial x_j}\left(\Gamma_\omega \frac{\partial \omega}{\partial x_j}\right) + G_\omega - Y_\omega + D_\omega + S_\omega \tag{2}$$

where $k$ is the turbulent kinetic energy; $\omega$ is the unit dissipation rate; $u_i$ is the average velocity component; $G_k$ and $G_\omega$ are the generations of the turbulence variables $k$ and $\omega$; $\Gamma_k$ and $\Gamma_\omega$ are the effective diffusivities of $k$ and $\omega$, respectively; $D_\omega$ is the orthogonal divergence term; $S_k$ and $S_\omega$ are the custom item; and $Y_k$ and $Y_\omega$ are the dissipative terms of $k$ and $\omega$, respectively.

### 2.4. Simulation Settings

With a flow rate of 55 L/min, the inlet boundary was set as the mass flow inlet. The static pressure value was set to atmospheric pressure, the wall condition was non-slip, and the two outlets were configured as pressure outlets. The impeller rotated at 3000 rpm. The unsteady calculation was carried out based on the results of the steady simulation, and the rotation field was set as "mesh motion". The time step for the transient calculation was set to $2.22 \times 10^{-4}$, which is equal to 1/90 T, according to the rotating period T of the impeller.

The volute and the impeller were also subjected to frame motion using the multiple reference frame (MRF) approach to simulate rotational motion. Additionally, the second-order upwind difference scheme was used during the discretization process, and the SIMPLE algorithm was utilized throughout the computation. The convergence residual was set to $10^{-4}$.

### 2.5. Experimental Validation

Figure 5 depicts the hydraulic performance test bench for the new type of dishwasher pump. It included a tank, a pump, an outlet pipeline, and an intake pipeline. The instrument location and the pipes leading from the outlet to the water tank were symmetrically placed, and the diameter of the volute outlet was 40 mm. Intelligent pressure sensors with an accuracy of 0.2% FS were used to measure the inlet and outlet pressure of the dishwasher pump, and the measuring range of pressure sensors was −20 kPa~20 kPa at the inlet and 0 kPa~30 kPa at the outlet.

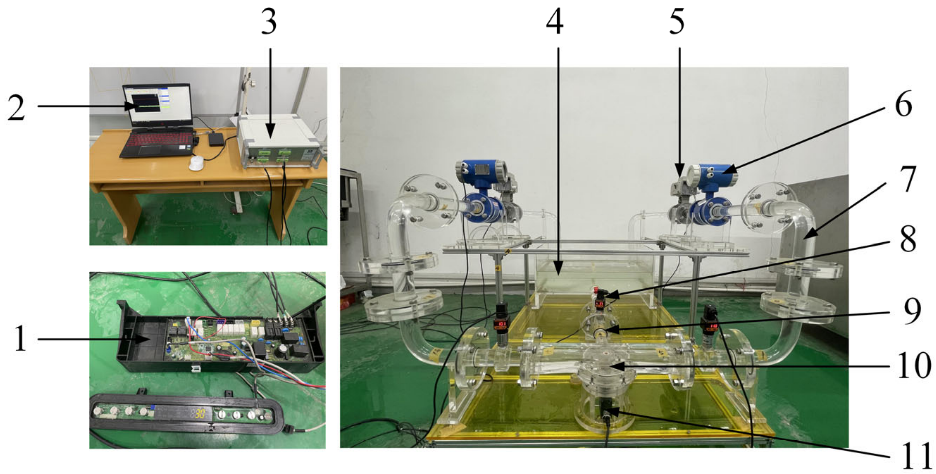


**Figure 5.** Hydraulic performance test bench for the new type of dishwasher pump. 1: motor speed controller, 2: computer, 3: data-acquisition system, 4: water tank, 5: electromagnetic valve, 6: turbine flowmeter, 7: outflow pipe, 8: pressure gauge, 9: inlet pipe, 10: dishwasher pump, and 11: torsiograph [1].

The flow rate was determined using an electromagnetic flowmeter with a 40 mm pipe diameter, 0.5% FS measurement accuracy, and a measuring range of 0.5 $m^3/h$ to 20 $m^3/h$. By manipulating the electromagnetic valve, the pump could be adjusted to a desirable operating condition, at which point the hydraulic characteristic curve of the dishwasher pump could be determined. An external electric actuator regulated the valve opening to guarantee the correctness of the regulation. The 0 to 1 opening of the solenoid valve was controlled with an electric actuator 0 to 100 with a flange connection. The measuring range of the torsiograph was 0 to 0.5 Nm with a 0.2% FS accuracy.

The head curve and efficiency curve of the original pump were obtained and are shown in Figure 4. According to the test results, as shown in Figure 6, the simulated curves revealed essentially compatible results with the experimental results. Under the design point, the error between the simulated efficiency and the experimental one was 8.3%, and the error between the simulated head and experimental value was 3.2%. The simulated head value under the low-flow scenario was higher than the test value, whereas the simulated efficiency value was lower than the test value, which fell within the error range of the numerical calculation.

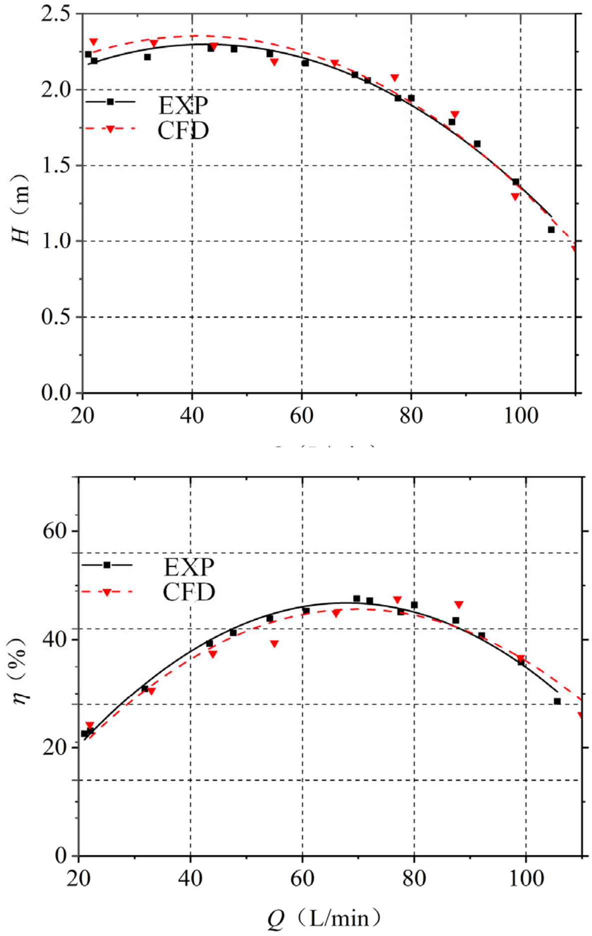


**Figure 6.** Comparison of simulated and experimental results.

## 3. Optimization Method and Parameters

As shown in Figure 7, an automatic optimization process was implemented for improvement in the efficiency of a new type of dishwasher pump by using Creo and ANSYS Workbench software. First, the complex twin-volute structure in the real machine was simplified, and the simplified twin-volute profile was controlled by six radii of curvature; the magnitude of these six radii of curvature was set as design variables. Second, within the boundaries of the design parameters, 100 twin-volute designs were generated using the Latin hypercube sampling (LHS) method and distributed at random throughout the designed space. Third, the simulation of these 100 cases was performed using ANSYS Fluent. Finally, optimization was based on sensitivity analysis and response surface optimization, which employed the MOGA method to iterate the twin-volute solution in search of the local optimal solution.

### 3.1. Design Parameters

As shown in Figure 3, the transformation from the volute structure to the mathematical model was made using the changes in the curvature radii of these six curves to characterize the structural alterations in the volute. Additionally, the initial curvature radius of the volute profile was used as the initial condition. The upper and lower ranges of each parameter, as indicated in Table 3, The upper and lower limits of the six input parameters were selected following the geometric principle, that is, they changed without affecting the general shape of the twin-volute, and the initial values were the average of the upper and lower limits.

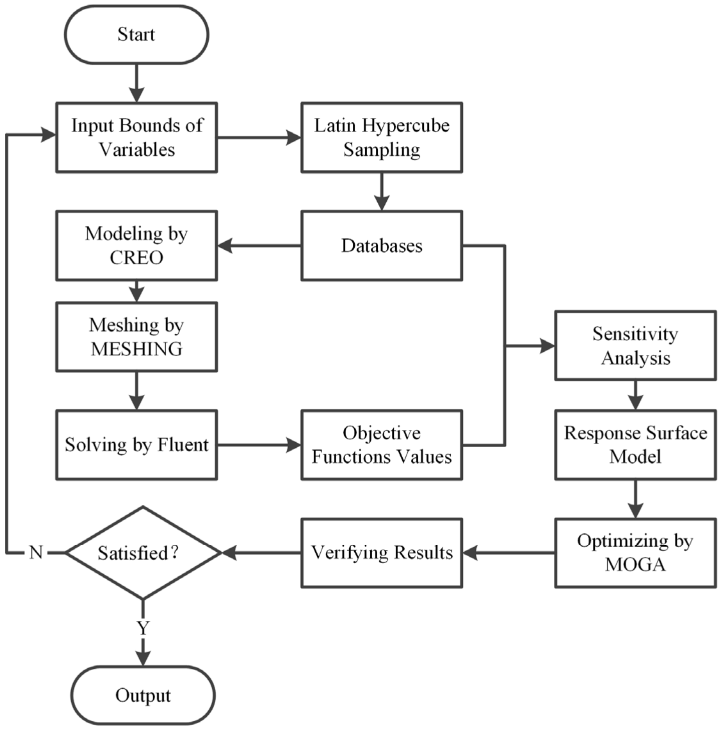


**Figure 7.** Optimization procedure.

**Table 3.** Initial values of each input parameter and their upper and lower limits.

| Parameters | DS_1 (mm) | DS_2 (mm) | DS_3 (mm) | DS_4 (mm) | DS_5 (mm) | DS_6 (mm) |
|---|---|---|---|---|---|---|
| Initial value | 70 | 380 | 180 | 120 | 50 | 29 |
| Upper limit | 100 | 560 | 260 | 170 | 70 | 30.5 |
| Lower limit | 40 | 200 | 100 | 70 | 30 | 27.5 |

### 3.2. Latin Hypercube Sampling

The Latin hypercube sampling method (LHS) was introduced in 1979 by McKay et al. [24] and was further developed by Iman Equal in 1981 [25]. LHS is an approximate random sampling method with multivariate parameter distribution and is among the stratified sampling techniques. It divides the sampling units into different layers according to a certain characteristic or a certain program and then independently and randomly extracts samples from different layers. In this way, the structure of the samples is relatively similar, and the accuracy of estimation is improved.

In total, 100 sampling points were randomly generated within the upper and lower limits of the parameters. Some combination data using LHS are shown in Table 4.

**Table 4.** Some of the input parameter data of 100 sample points.

| NO. | DS_1 (mm) | DS_2 (mm) | DS_3 (mm) | DS_4 (mm) | DS_5 (mm) | DS_6 (mm) |
|---|---|---|---|---|---|---|
| 1 | 57.7 | 493.4 | 140.8 | 165.5 | 60.6 | 28.895 |
| 2 | 72.1 | 331.4 | 107.2 | 90.5 | 41.8 | 27.905 |
| 3 | 40.9 | 234.2 | 168 | 134.5 | 36.2 | 30.005 |
| 4 | 64.3 | 551 | 132.8 | 154.5 | 66.2 | 28.775 |
| ... | ... | ... | ... | ... | ... | ... |
| 97 | 49.3 | 396.2 | 123.2 | 164.5 | 46.6 | 29.825 |
| 98 | 70.9 | 540.2 | 105.6 | 81.5 | 53.8 | 30.425 |
| 99 | 81.1 | 259.4 | 185.6 | 94.5 | 54.6 | 29.735 |
| 100 | 71.5 | 407 | 176 | 142.5 | 55 | 28.745 |

### 3.3. Optimization Objective

In this study, the head and efficiency values of the dishwasher pump were taken as the optimization objectives. Equations (3) and (4) present the expressions of the head and efficiency of the dishwasher pump, respectively. The efficiency was chosen as the first optimization target, while Max ($\eta$), i.e., the maximum efficiency value with no lower bound, served as the constraint. The head of the dishwasher pump was set as the optimization objective, and the constraint condition was $H \geq 2$ m to meet the design head. Finally, the three ideal samples satisfying the constraint conditions were selected.

$$H = (P_{out} - P_{in})/\rho g \tag{3}$$

where $H$ is the head of the pump (m); $P_{out}$ and $P_{in}$ are the total pressure of the pump outlet and inlet, respectively (Pa); $\rho$ represents the water density (kg/m$^3$); and $g$ is the gravitational acceleration (N/kg).

$$\eta = \rho g Q H/P \tag{4}$$

where $\eta$ is the efficiency of the pump (%); $Q$ represents the mass flow rate (kg/s); and $P$ is the shaft power (W).

### 3.4. Response Surface Method

Response surface method is a statistical method to study the relationship between the objective function and the design parameters. The RSM method was first introduced by Box and Wilson [26]. While Latin hypercube sampling design and central composite design are the most commonly used experimental design methods, and they form the basis of the response surface methodology, as mentioned before, Latin hypercube sampling design was also considered in the present research. The genetic aggregation method is often selected as RSM [27,28]. Wang et al. [29] pointed out that genetic aggregation methods are more reliable than other metamodels by performing cross-validation and multiple solutions of the response surface. This approach basically constitutes the following response surface.

$$\hat{y}_{ens}(x) = \sum_{i=1}^{N_m} w_i \cdot \hat{y}_i \tag{5}$$

where $x$ and $y$ are the estimates of the population, and $i$ is the $i$th response, respectively. $N_m$ and $w$ are the number of metamodels and the weight factor of the $i$th response, respectively.

### 3.5. Multi-Objective Genetic Algorithm

For multi-objective problems, it is nearly impossible to acquire a solution that optimizes all objective functions. Thus, the Pareto-optimal solution was used in this study. To obtain the Pareto frontier for the two objective functions, a multi-objective genetic algorithm (MOGA) [30] was also considered in the present study.

The global parameters of the algorithm for this study are shown in Table 5. After calculating the fitness of each individual under different design parameters, the Pareto frontier for each iteration including the initial population was updated. Since there is more than one objective function, the individual cannot be evaluated by the value of each function. To solve this problem, the following formula was used to evaluate individuals.

$$f(\alpha) = \frac{1}{1 + \|\alpha - \beta\|_2} \tag{6}$$

where $\alpha$ is any individual in the population; $\beta$ is the Pareto efficient individual located nearest $\alpha$; and $\|\alpha - \beta\|_2$ is the Euclidean distance between these two individuals.

**Table 5.** Parameters adopted in MOGA.

| Parameters | Value |
|---|---|
| Number of initial samples | 6000 |
| Number of samples per iteration | 1200 |
| Maximum allowable Pareto percentage | 70 |
| Convergence stability percentage | 2 |
| Maximum number of iterations | 20 |

According to the Equation (6), only the individuals located on the Pareto frontier can make the assessed value equal to one, and this figure will be smaller if the individuals go farther. As depicted in Figure 8, when the number of iterations reached 5, the percentage of convergence stability was less than 2%, and the calculation stopped.

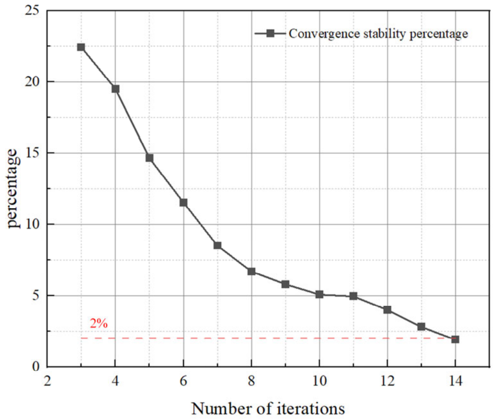


**Figure 8.** Convergence figure for the MOGA.

## 4. Result and Discussion

### *4.1. Optimization Parameter Analysis*

#### 4.1.1. Sensitivity Analysis

The local sensitivity of the six input parameters of the twin-volute design relative to its two output parameters (head and efficiency) is given in Figure 9. As can be seen, the change in the input parameter "DS_6" was the most sensitive to the head and efficiency of the dishwasher pump, which means that even a small change in the input parameter "DS_6" would result in a significant change in the output parameter, whereas the change in the input parameter "DS_3" was the least sensitive.

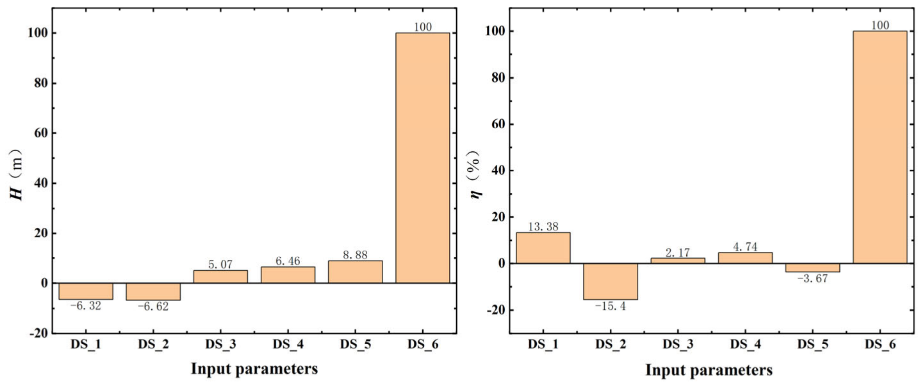


**Figure 9.** Local sensitivity diagram. (**a**) Local sensitivity of the head and (**b**) local sensitivity of the efficiency.

Therefore, during the optimization process, the upper and lower limits of the input parameter "DS_6" could be appropriately compressed, and the sampling interval of the input parameter with lower sensitivity could be properly expanded, which resulted in a more thorough selection of the test samples. These two parameters were more sensitive to efficiency when compared to how responsive the input parameters "DS_1" and "DS_2" were to the head. The input parameters "DS_3", "DS_4", and "DS_5", on the other hand, were less sensitive to efficiency than to the head. The three input parameters "DS_1", "DS_2", and "DS_6" were considered the main optimal targets in this study because efficiency was taken as the primary optimization objective.

#### 4.1.2. Response Surface Analysis

The response surface of the paired parameter on the head was examined, and the corresponding response curve was constructed, to more intuitively investigate the influence of each parameter on the hydraulic performance of the dishwasher pump. The six input parameters for the twin-volute structure were determined, and their effects on the dishwasher pump head are depicted in Figure 10.

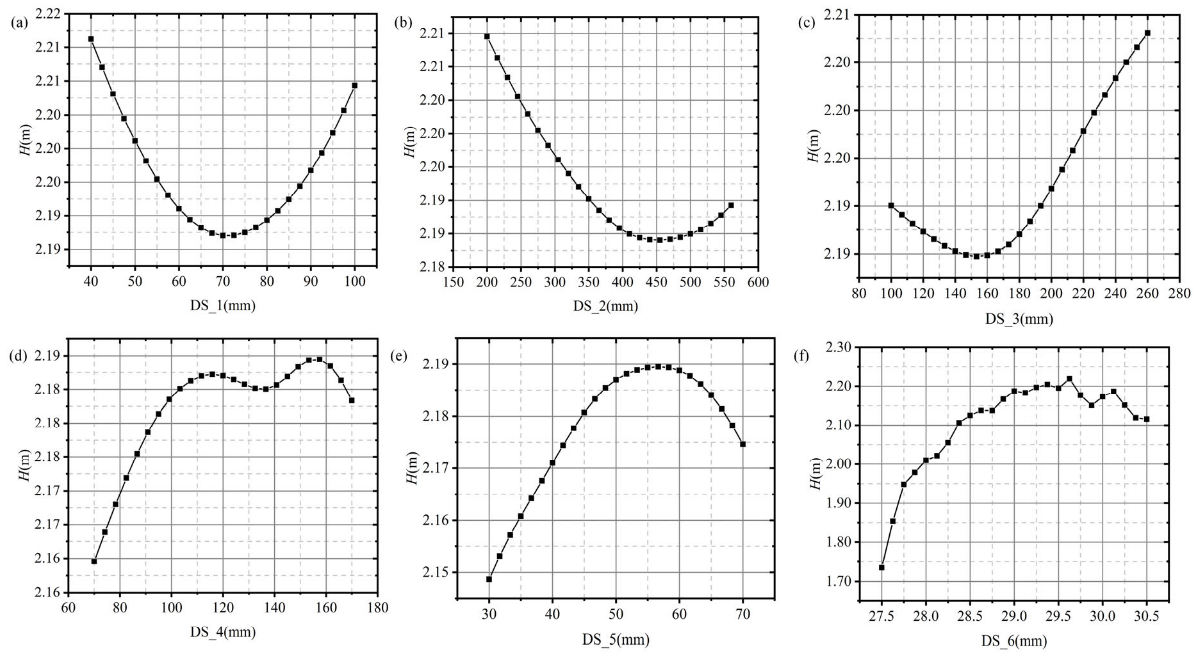


**Figure 10.** Effect of design variables on the head: (**a**) DS_1, (**b**) DS_2, (**c**) DS_3, (**d**) DS_4, (**e**) DS_5, and (**f**) DS_6.

The same tendency was observed in the fluctuation of the head for the input parameters "DS_1", "DS_2", and "DS_3". In other words, the head declined and subsequently increased when the parameter valve was increased, and the curves were smooth. However, the input parameter "DS_5" had a reverse effect from the above. As the input parameter "DS_4" increased in the sample interval, the change in the head showed a fluctuation. With the increase in the input parameter "DS_6", in comparison to the previous five parameters, the head of the curve trend was more disordered, and the curves were no longer smooth. It is important to note that, when the input parameter "DS_6" changed, the variable range of the head increased, and its lower limit fell even closer to 1.75 m, supporting the notion that the input parameter "DS_6" was the most sensitive parameter to the head.

Figure 11 shows the impact of the six twin-volute input parameters on the efficiency of the dishwasher pump. The impact of input parameters on the efficiency of the dishwasher pump can be simply and intuitively understood, which suggests how to further optimize the twin-volute design. To achieve higher pump efficiency, the selected interval of the parameter "DS_1" value should be greater than 100 mm or less than 40 mm. The value of parameter "DS_2" should be less than 200 mm; the selection interval of parameter "DS_3" value should be between 220 mm and 230 mm; the selection range of parameter "DS_4" value should be between 150 mm and 160 mm; the selection range of parameter "DS_5" value should be between 45 mm and 50 mm, and the value of parameter "DS_6" should be around 29.5 mm. With these optimal parameters, the efficiency of the pump can be increased. The selection interval for each input parameter can be further defined through the preliminary sample analysis, which serves as a foundation for choosing the sample database for the optimization.

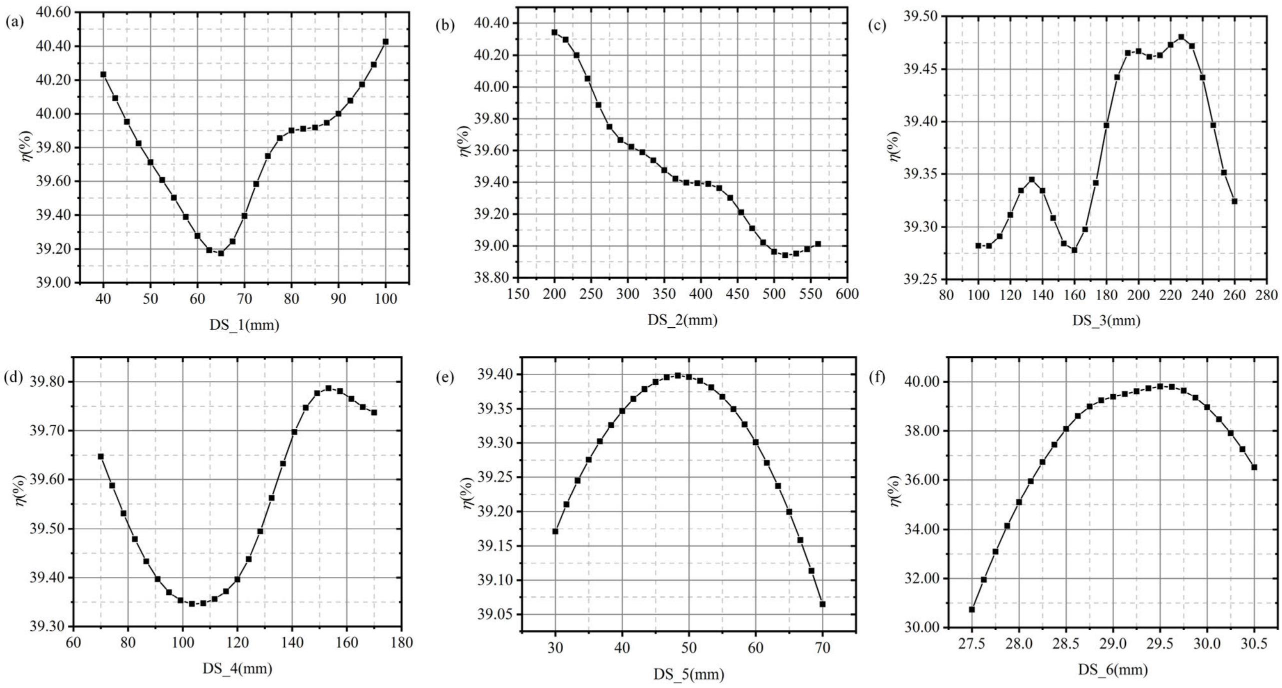


**Figure 11.** Effect of design variables on efficiency: (**a**) DS_1, (**b**) DS_2, (**c**) DS_3, (**d**) DS_4, (**e**) DS_5, and (**f**) DS_6.

*4.2. Comparison of Hydraulic Performance before and after Optimization*

For optimization issues involving discrete variables, the genetic algorithm (GA) is a practical and quick global parallel stochastic optimization search tool. In this study, based on the idea of a controlled elite, the multi-objective genetic algorithm (MOGA) and a variation in the non-dominated sorting genetic algorithm II (NSGA-II) were chosen for optimization. This approach supports various goals and restrictions and seeks to identify the most ideal answer.

As shown in Table 6, three optimal samples were found by using MOGA. All three examples had higher heads than the original heads. As a result, the most effective candidate was chosen as the best choice. In this scheme, the twin-volute dishwasher pump had a head of 2.2099 m and an efficiency of 42.13%. The two-dimensional comparison diagram of the twin-volute profile is given in Figure 12 and is based on the values of each parameter of the twin-volute profile before and after optimization.

**Table 6.** Optimal results.

| Parameter | The Original Model | Candidate 1 | Candidate 2 | Candidate 3 |
|---|---|---|---|---|
| DS_1 (mm) | 70 | 99.72 | 99.899 | 98.907 |
| DS_2 (mm) | 380 | 200.01 | 209.1 | 203.52 |
| DS_3 (mm) | 180 | 101.88 | 101.74 | 140.29 |
| DS_4 (mm) | 120 | 70.479 | 71.472 | 148.52 |
| DS_5 (mm) | 50 | 48.492 | 51.779 | 64.542 |
| DS_6 (mm) | 29 | 29.182 | 29.165 | 28.912 |
| $\eta$ (%) | 39.396 | 42.13 | 42.063 | 42.052 |
| $H$ ($m$) | 2.187 | 2.2099 | 2.1985 | 2.2646 |

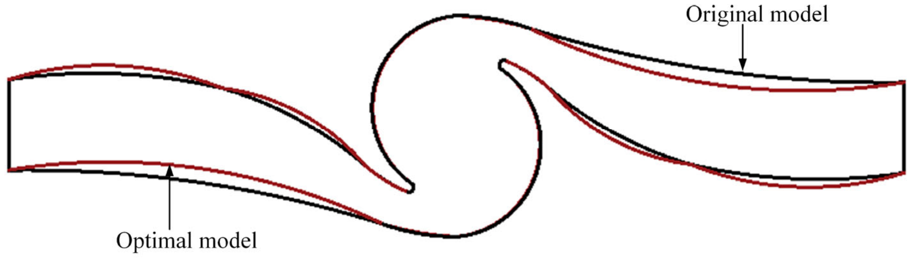


**Figure 12.** Comparison of the profile of twin-volute before and after optimization.

Figure 13 compares the hydraulic performance of the twin-volute schemes (as shown in Figure 12) before and after optimization. The pump head and efficiency of the optimal twin-volute model were improved under all conditions. By contrast, the deviation of the efficiency curve of the optimal model from that of the original model fell first and subsequently increased, and the deviation of the head curve of the optimal model from that of the original model steadily increased as the flow rate increased. Under the design point, the head slightly changed before and after optimization, while the efficiency significantly increased, showing an increase of 2.7%. In addition, the difference was the greatest around the flow rate of 99 L/min and was at least near the flow rate of 50 L/min.

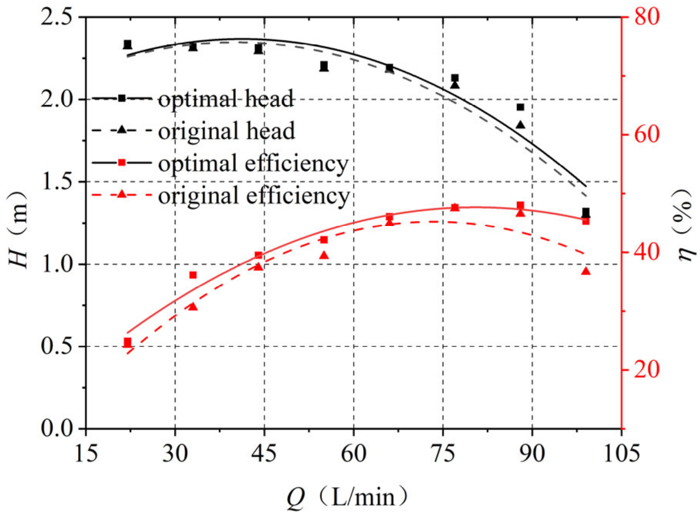


**Figure 13.** Comparison of pump characteristics before and after optimization.

### 4.3. Comparison of Inflow Characteristics before and after Optimization

As shown in Figure 14, the channels of the impeller, four toroidal surfaces were selected in the blade radial direction based on the central axis of the impeller, which passed through the bottom and top of the impeller, and the axial surface of each torus was expanded to facilitate a more intuitive observation of the distribution of turbulent kinetic energy.

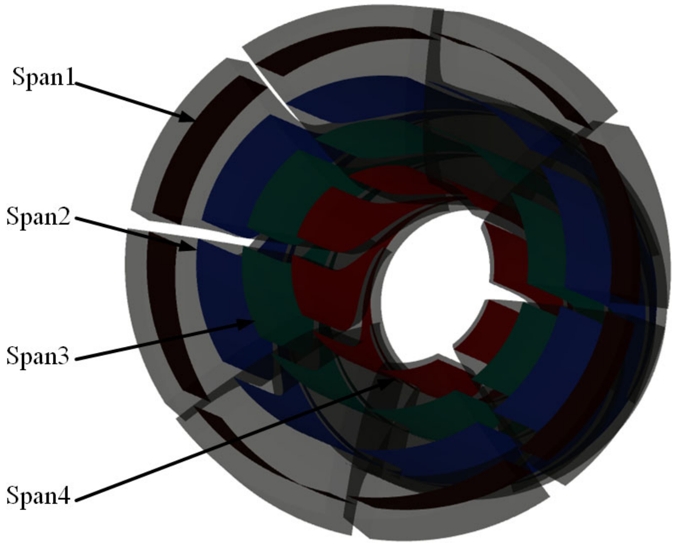


**Figure 14.** Schematic diagram of the plane expansion.

As shown in Figure 15, four concentric circles, defined as $C_0$, $C_1$, $C_2$, and $C_3$, were selected from the outlet of the impeller to the inlet of the impeller, and the outer rings of the circles fell on the midline of the flow channels of the impeller. In addition, each flow channel of the impeller was also defined, and the symmetrical flow channel 1 and flow channel 5 were closed to the two tongues of the twin-volute pump.

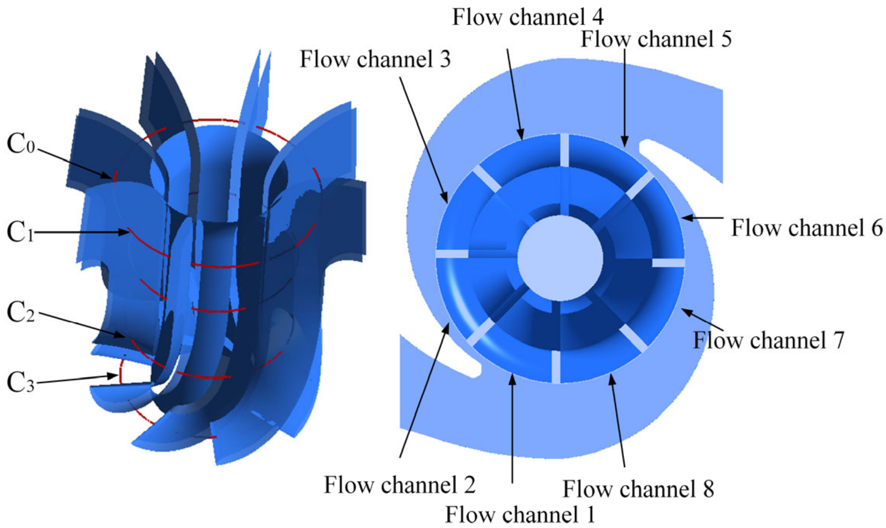


**Figure 15.** Schematic diagram of impeller flow channel distribution.

The turbulent kinetic energy distribution on the four toroidal surfaces in the impeller of the twin-volute pump before and after optimization are compared in Figure 16. Figure 16a demonstrates that, in both the original and optimal models, the turbulent kinetic energy in the Span1 plane of the dishwasher pump impeller was primarily distributed at the outlet of the impeller, demonstrating that turbulent vortices were more intense during the flow transition from the impeller to the volute. From Figure 16b, it can be inferred that, when the impeller flow channel was close to the two-volute tongues, the turbulent kinetic energy in the fourth and eighth channels of the impeller gradually increases from the inlet to the outlet of the impeller, while the turbulent kinetic energy in the other channels of the impeller that were not located at the volute tongue was primarily concentrated in the middle part of the impeller. It can be seen from Figure 16c that the water flow in the impeller channels fully developed and became more complex as the annular surface of the impeller moved away from the hub of the impeller, and the turbulent kinetic energy gradually filled the entire impeller channels. As a result, a relatively high turbulent kinetic energy distribution also appeared in the area of the leading edge of the blade inlet. Figure 16d demonstrates that, while the turbulent kinetic energy of the optimal model was significantly higher than that of the original model in some impeller channels, such as channels 4 and 8, it was significantly lower in those positions close to the volute tongue. Nevertheless, the optimal model was more effective in lowering the gradient of the impeller channels. As a result, the turbulent kinetic energy distribution became more uniform. In conclusion, the impeller of the optimal model had a lower overall distribution of the turbulent kinetic energy than the original model, which contributed to a reduction in the hydraulic loss of the impeller and an increase in the overall efficiency of the pump.

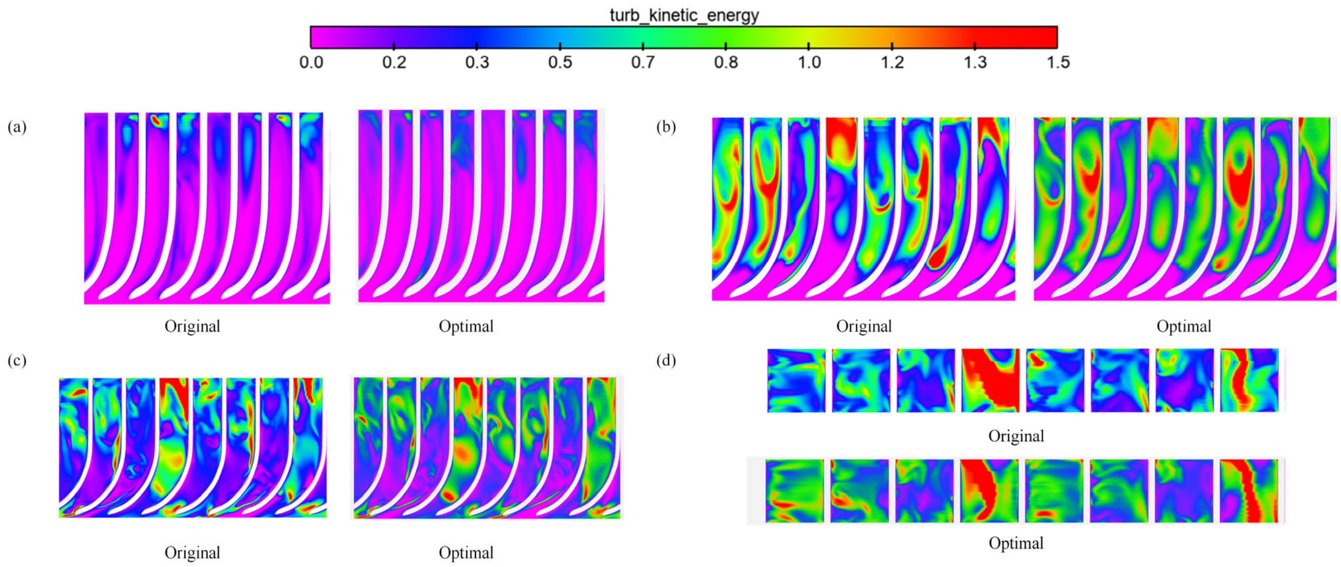


**Figure 16.** Turbulent kinetic energy contours on the expanded plane: (**a**) Span1, (**b**) Span2, (**c**) Span3, (**d**) Span4.

The pressure profile in the flow channels of the model impeller before and after optimization is given in Figure 17. Figure 17a–c shows that, except for channels 1 and 5, which are close to the volute tongue, the pressure on the blade pressure side in the majority of impeller channels was higher than the pressure on the suction surface. Figure 17d, however, reveals the opposite result at the impeller inlet position. In contrast to Figure 17a,d, the pressure distribution in the flow channels was similar in positions close to the impeller inlet and regularly changed. The difference in the pressure distribution between each of the flow channels of the impeller became gradually apparent as it approached the position of the impeller output. The impeller outlet flow pattern became complex as a result of the interference between the volute and impeller, and the flow of uncertainty increased. The pressure in each flow channel of the impeller was higher after optimization, and the closer to the impeller outlet, the greater the pressure difference before and after optimization, as is evident from the pressure distribution in channels 1 and 5. This can be verified by comparing the models before and after optimization.

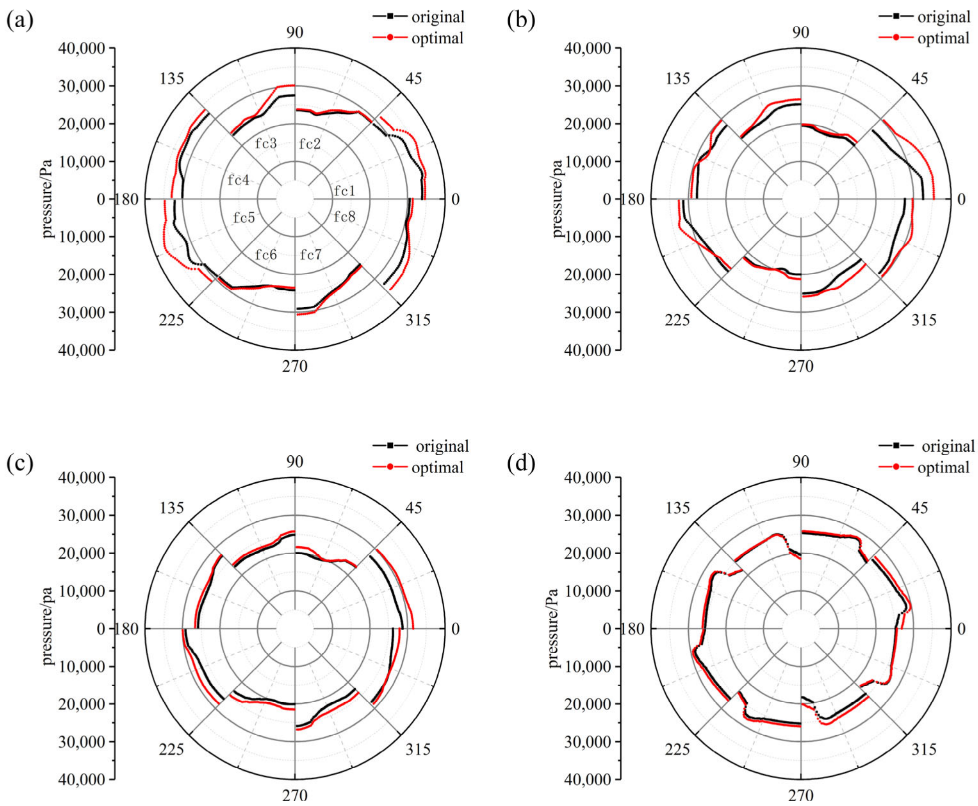


**Figure 17.** Pressure distribution diagram of impeller runner (**a**) C0, (**b**) C1, (**c**) C2, and (**d**) C3.

Figure 18 shows the velocity vector comparison diagram on the middle section of the twin-volute pump before and after optimization. Figure 18 demonstrates that the interaction between the impeller and the volute on the flow pattern resulted in a localized high-speed area at the location of the twin-volute tongues. The velocity gradually dropped as water moved downstream of the volute channel, presumably as a result of the expansion of the flow area via the volute.

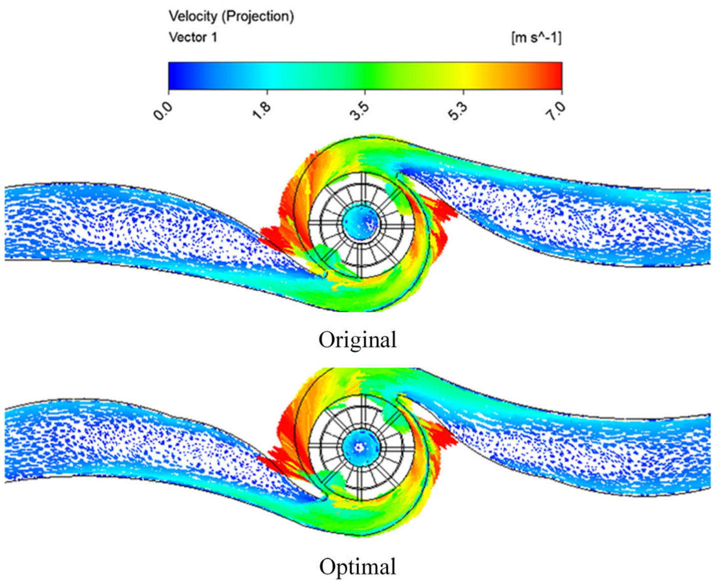


**Figure 18.** Velocity vector diagram of the middle section of the volute.

According to Figure 19, the vortices in the twin-volute model were primarily distributed in the outlets of eight blades and two tongues, with a significant number of wall vortices also being produced on the volute wall. The vortices downstream of the volute gradually diminished as the vortices formed and shed themselves. The optimal model efficiently reduced the vorticity in the volute inlet area and decreased the hydraulic loss, demonstrating that it is more efficient than the original model.

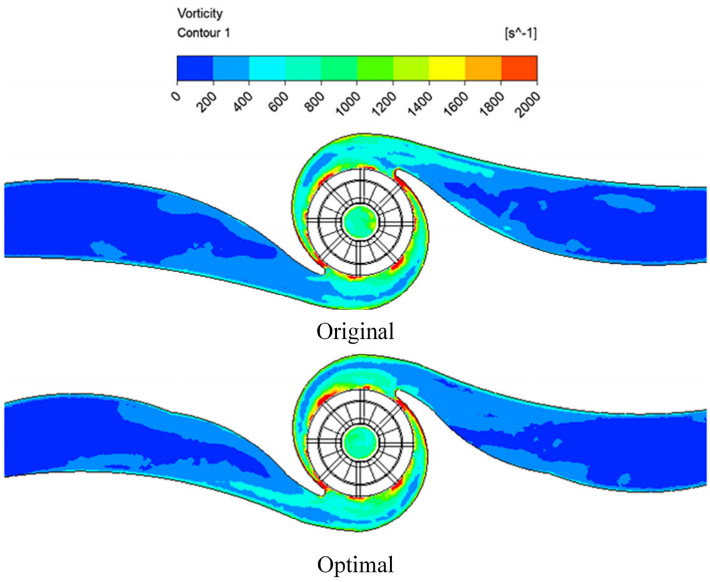


**Figure 19.** Vorticity contours of the middle section of the volute.

Figure 20 depicts the linear position diagram parallel to the top of the twin-volute structure and running along the outlet direction to examine the pressure changes from the volute tongue position to the outlet after the water passed through the new type of dishwasher pump. The pressure distribution on each line was analyzed as follows:

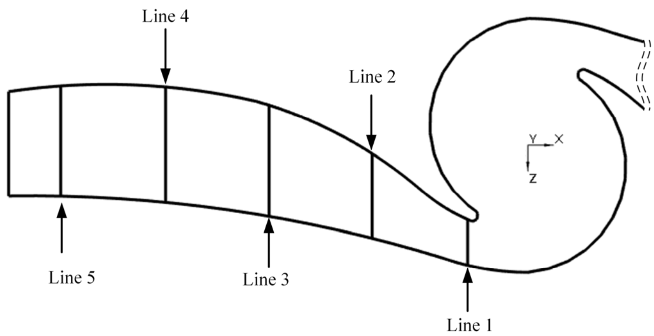


**Figure 20.** Schematic diagrams of the straight line position along the volute outlet flow channel.

Figure 21a demonstrates how the water flow collided and extruded with the tongue as it passed through the impeller, causing the pressure to rapidly drop in those places closer to the tongue and gradually change with more distance. By comparing Figure 21b,c, it can be seen that the highest pressure was close to the outside wall of the volute, and the minimum pressure was close to the inner wall. The pressure gradient steadily increased as the water flow downstream developed, and this characteristic is also evident at the intersection of Lines 4 and 5. Figure 21d,e shows that the pressure trend is parabolic in general. The pressure was minimal close to the walls on either side of the volute and was greatest in the flow channel in the center of the volute. Overall, the optimal twin-volute structure ensured the enhancement of the pump pressure since the pressure of the optimal model at each point was higher than that of the original model.

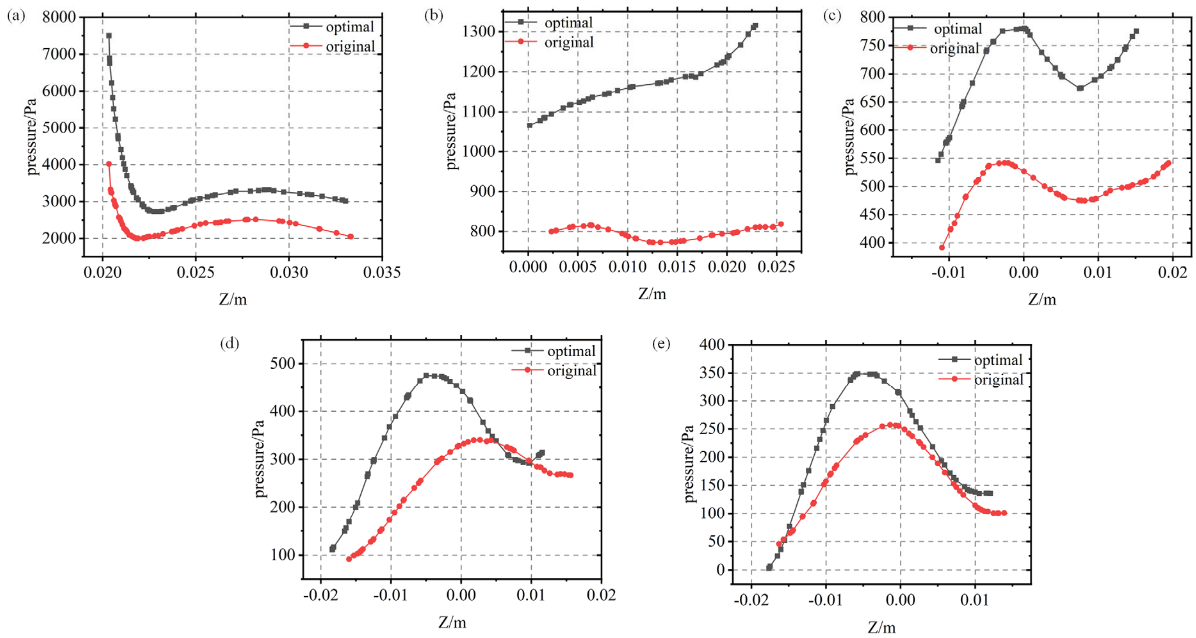


**Figure 21.** Pressure distribution on the middle section of the volute (**a**) Line 1, (**b**) Line 2, (**c**) Line 3, (**d**) Line 4, and (**e**) Line 5.

## 5. Conclusions

An automatic numerical optimization method that combined the RSM and MOGA was proposed to improve the efficiency of the new type of dishwasher pump. The numerical simulation results with SST $k$–$\omega$ turbulence models were evaluated and verified through experiments. The database of the twin-volute structure controlled by six radii of curvature was generated with LHS. The response surface optimization method (RSM) was crucial in choosing the parameter interval for the optimization, and the MOGA allowed for choosing a more effective hydraulic model. By comparing and analyzing the numerical simulation results of the model before and after optimization, the following conclusions can be drawn:

(1) The "DS_6" parameter representing the external profile of the first to the fourth section of the worm shell had the most significant effect on the pump head and efficiency, which provided the basis for the selection of the interval size in the optimization, and the results of the response surface optimization provided a solution for the selection of the parameter interval range in the optimization;

(2) The head flow curves did not significantly change before and after optimization. By contrast, the optimal efficiency significantly changed, with a 2.7% increase in the efficiency at the design point;

(3) Compared with the original model, the impeller of the optimal model pump had a lower overall distribution of turbulent kinetic energy and higher overall pressure in its flow channels. The optimal model efficiently reduced the vorticity in the twin-volute inlet area and increased the pressure in the flow channel. All the above findings confirmed that the optimal model had better hydraulic performance than the original model;

(4) The combination of the RSM and MOGA can effectively solve the problem of optimization for new types of dishwashers and provides a reference for the development of subsequent hydraulic models.

**Author Contributions:** Conceptualization, H.S. and H.X.; methodology, H.S.; software, H.S. and Y.L. (Yanjun Li); validation, H.X., X.W. and Y.L. (Yalin Li); formal analysis, H.S.; data curation, H.S.; writing—original draft preparation, H.S.; writing—review and editing, Y.L. (Yanjun Li), X.W. and Y.L. (Yalin Li) All authors have read and agreed to the published version of the manuscript.

**Funding:** This research was funded by the Natural Science Foundation of Jiangsu Province (No. BK20180871), the project of National Natural Science Foundation of China (No. 51809120), the

Project Funded by China Postdoctoral Science Foundation (No. 2018M640462), the Natural Science Foundation of the Jiangsu Higher Education Institutions of China (No. 18KJB470005), and the Priority Academic Program Development of Jiangsu Higher Education Institutions (PAPD).

**Conflicts of Interest:** The authors declare no conflict of interest.

## References


1. Li, Y.; Sun, H.; Xu, H.; Wang, X.; Li, Y. Orthogonal Optimization Design of the Compound Impeller for a New Type of Dishwasher Pump. *Processes* **2022**, *10*, 1813. [CrossRef]
2. Ning, C.; Li, Y.; Huang, P.; Xu, H.; Zheng, F. Numerical Analysis of a New Type of Dishwasher Pump for Different Rotation Speeds of the Volute. *Front. Energy Res.* **2022**, *9*, 825159. [CrossRef]
3. Zhu, Y.; Zhang, J.; Li, Y.; Huang, P.; Xu, H.; Zheng, F. Experimental Investigation of Unsteady Pressure Pulsation in New Type Dishwasher Pump with Special Double-Tongue Volute. *Machines* **2021**, *9*, 288. [CrossRef]
4. Zhang, J.; Zhu, Y.; Li, Y.; Huang, P.; Xu, H.; Zheng, F. Investigation of Unsteady Pressure Pulsation in New Type Dishwasher Pump with Special Double Tongue Volute. *Shock Vib.* **2022**, *2022*, 9349432. [CrossRef]
5. Kaupert, K.A.; Staubli, T. The Unsteady Pressure Field in a High Specific Speed Centrifugal Pump Impeller—Part I: Influence of the Volute. *J. Fluids Eng.* **1999**, *121*, 621–626. [CrossRef]
6. Hodkiewicz, M.R.; Norton, M.P. The effect of change in flow rate on the vibration of double-suction centrifugal pumps. *Proc. Inst. Mech. Eng. Part E J. Process. Mech. Eng.* **2002**, *216*, 47–58. [CrossRef]
7. Chu, S.; Dong, R.; Katz, J. Relationship Between Unsteady Flow, Pressure Fluctuations, and Noise in a Centrifugal Pump—Part B: Effects of Blade-Tongue Interactions. *J. Fluids Eng.* **1995**, *117*, 30–35. [CrossRef]
8. Shi, L.; Yuan, Y.; Jiao, H.; Tang, F.; Cheng, L.; Yang, F.; Jin, Y.; Zhu, J. Numerical investigation and experiment on pressure pulsation characteristics in a full tubular pump. *Renew. Energy* **2021**, *163*, 987–1000. [CrossRef]
9. Zhang, F.; Lowys, P.; Houdeline, J.; Guo, X.; Hong, P.; Laurant, Y. Pump-turbine Rotor-Stator Interaction Induced Vibration: Problem Resolution and Experience. *IOP Conf. Series: Earth Environ. Sci.* **2021**, *774*, 012124. [CrossRef]
10. Song, X.; Liu, C. Experimental investigation of pressure pulsation induced by the floor-attached vortex in an axial flow pump. *Adv. Mech. Eng.* **2019**, *11*, 1687814019838708. [CrossRef]
11. Ateş, H.; Engineer, A.C.M.; Ateş, F. A geometrical model of dishwasher spray arm for CornerWash. *AIMS Math.* **2022**, *7*, 8534–8541. [CrossRef]
12. Dedoussis, V.; Giannatsis, J. Stereolithography assisted redesign and optimisation of a dishwasher spraying arm. *Rapid Prototyp. J.* **2004**, *10*, 255–260. [CrossRef]
13. Wu, D.; Yuan, S.; Ren, Y.; Mu, J.; Yang, Y.; Liu, J. CFD investigation of the influence of volute geometrical variations on hydrodynamic characteristics of circulator pump. *Chin. J. Mech. Eng.* **2016**, *29*, 315–324. [CrossRef]
14. De Donno, R.; Ghidoni, A.; Noventa, G.; Rebay, S. Shape optimization of the ERCOFTAC centrifugal pump impeller using open-source software. *Optim. Eng.* **2019**, *20*, 929–953. [CrossRef]
15. Remo, D.; Stefano, R.; Ghidoni, A. Surrogate-Based Shape Optimization of the ERCOFTAC Centrifugal Pump Impeller. In *Evolutionary and Deterministic Methods for Design Optimization and Control with Applications to Industrial and Societal Problems*; Springer: Cham, Switzerland, 2019; pp. 227–246. [CrossRef]
16. De Donno, R.; Fracassi, A.; Ghidoni, A.; Congedo, P.M. Uncertainty Assessment of an Optimized ERCOFTAC Pump. In *Advances in Evolutionary and Deterministic Methods for Design, Optimization and Control in Engineering and Sciences*; Springer: Cham, Switzerland, 2021; pp. 191–209. [CrossRef]
17. Thakkar, S.; Vala, H.; Patel, V.K.; Patel, R. Performance improvement of the sanitary centrifugal pump through an integrated approach based on response surface methodology, multi-objective optimization and CFD. *J. Braz. Soc. Mech. Sci. Eng.* **2021**, *43*, 24. [CrossRef]
18. Lu, R.; Yuan, J.; Wei, G.; Zhang, Y.; Lei, X.; Si, Q. Optimization Design of Energy-Saving Mixed Flow Pump Based on MIGA-RBF Algorithm. *Machines* **2021**, *9*, 365. [CrossRef]
19. Zhao, X.; Zhang, D.; Zhang, R.; Xu, B. A comparative study of Gaussian process regression with other three machine learning approaches in the performance prediction of centrifugal pump. *Proc. Inst. Mech. Eng. Part C J. Mech. Eng. Sci.* **2022**, *236*, 3938–3949. [CrossRef]
20. Wang, W.; Pei, J.; Yuan, S.; Zhang, J.; Yuan, J.; Xu, C. Application of different surrogate models on the optimization of centrifugal pump. *J. Mech. Sci. Technol.* **2016**, *30*, 567–574. [CrossRef]
21. Zhang, R.; Chen, X.; Luo, J. Knowledge Mining of Low Specific Speed Centrifugal Pump Impeller Based on Proper Orthogonal Decomposition Method. *J. Therm. Sci.* **2021**, *30*, 840–848. [CrossRef]
22. Chen, X.; Zhang, R.; Jiang, L.; Yang, W. Adaptive POD surrogate model method for centrifugal pump impeller flow field reconstruction based on clustering algorithm. *Mod. Phys. Lett. B* **2021**, *35*, 2150126. [CrossRef]
23. Menter, F.R. Two-equation eddy-viscosity turbulence models for engineering applications. *AIAA J.* **1994**, *32*, 1598–1605. [CrossRef]
24. McKay, M.D.; Beckman, R.J.; Conover, W.J. A Comparison of Three Methods for Selecting Values of Input Variables in the Analysis of Output from a Computer Code. *Technometrics* **2000**, *42*, 55–61. [CrossRef]

25. Iman, R.L.; Helton, J.C.; Campbell, J.E. An Approach to Sensitivity Analysis of Computer Models: Part I—Introduction, Input Variable Selection and Preliminary Variable Assessment. *J. Qual. Technol.* **1981**, *13*, 174–183. [CrossRef]
26. Box, G.E.P.; Wilson, K.B. On the Experimental Attainment of Optimum Conditions. *J. R. Stat. Soc. Ser. B Methodol.* **1951**, *13*, 1–38. [CrossRef]
27. Acar, E. Various approaches for constructing an ensemble of metamodels using local measures. *Struct. Multidiscip. Optim.* **2010**, *42*, 879–896. [CrossRef]
28. Viana, F.; Haftka, R.T.; Steffen, V. Multiple surrogates: How cross-validation errors can help us to obtain the best predictor. *Struct. Multidiscip. Optim.* **2009**, *39*, 439–457. [CrossRef]
29. Wang, S.; Jian, G.; Xiao, J.; Wen, J.; Zhang, Z. Optimization investigation on configuration parameters of spiral-wound heat exchanger using Genetic Aggregation response surface and Multi-Objective Genetic Algorithm. *Appl. Therm. Eng.* **2017**, *119*, 603–609. [CrossRef]
30. Gen, M.; Cheng, R. *Genetic Algorithms and Engineering Optimization*; John Wiley & Sons, Inc.: New York, NY, USA, 1999.